Thesis for the degree of Licentiate of Engineering

Hydrogen Fuel Cell Aircraft for Regional Travel

Christian Svensson

Department of Mechanics and Maritime Sciences
CHALMERS UNIVERSITY OF TECHNOLOGY
Göteborg, Sweden 2024

Hydrogen Fuel Cell Aircraft for Regional Travel
Christian Svensson

Licentiatavhandlingar vid Chalmers tekniska högskola
Technical report No. 2024:11

Department of Mechanics and Maritime Sciences
Chalmers University of Technology
SE–412 96 Göteborg, Sweden
Telephone + 46 (0) 31 – 772 1000

Chalmers Reproservice
Göteborg, Sweden 2024

To my loving and supportive family.

Abstract

Hydrogen Fuel Cell Aircraft for Regional Travel
Christian Svensson
Division of Fluid Dynamics, Department of Mechanics and Maritime Sciences
Chalmers University of Technology

With ever increasing travel demand, with some projections estimating a two-fold increase of passenger volume in 2050, the efficiency gains made in conventional aircraft designs are simply not keeping up with the pace of increasing emissions. A possible way to de-carbonize regional air travel is through the use of fuel cell aircraft, which are electric aircraft with liquid hydrogen as its energy-carrier.

Hydrogen carries roughly three times the energy per mass compared to conventional jet-fuel, but is of much lower density and therefore needs large storage volumes. The liquid hydrogen is a cryogenic, and therefore requires specialized insulated pressure vessels, which adds weight. Additionally, due to the low system specific power of fuel cells, the total aircraft weight will increase compared to a turboprop counterpart. On the flip-side, a fuel cell system has a comparatively high efficiency, and can therefore offset the negative performance aspects brought on by the system.

In this thesis, methods for conceptually designing and simulating the mission performance of regional fuel cell aircraft are presented. These produce representative airframes and propulsive systems that then can be used for studying the aircraft's performance, in areas such as the impact of choices made in the cryogenic storage design.

In the first appended paper, a regional fuel cell aircraft was sized for Nordic market requirements and its cryogenic storage evaluated in two different types of flight operation. For the conventional design mission, a tank with moderate ventilation pressure and high insulation layer count struck the best balance between weight and boil-off losses. For the return-without-refuel mission, the tank with a high ventilation pressure and high insulation count minimized boil-off losses and outperformed the lighter tanks for groundhold times in excess of 2 hours.

The second paper covers the integration of sizing and mission methods into SUAVE. This includes a routine for sizing the cooling system using a conceptual design heat-exchanger code. Additionally, the procedure for performing redesigns of existing turboprop aircraft is described. An ATR 42 is redesigned for fuel cell propulsion which requires airframe resizing due to increased weight and the cryostorage. For 6 m^3 of fuel the take-off weight increased by 6% and exhibits a 5.5% MAC centre-of-gravity shift between full and empty conditions.

Keywords: conceptual aircraft design, liquid hydrogen, proton-exchange membrane fuel cell, cryogenic storage, short-range, regional

Acknowledgments

The work carried out in this project would not have been possible without the funding from the research center TechForH_2 and the support from the people around me. I would like to thank my supervisor Tomas Grönstedt for giving me this opportunity, but maybe most importantly for being a nice person and sharing his wealth of knowledge within aeronautics and dad-jokes. My examiner plus the both official and unofficial co-supervisors have also been of great support. To Niklas Andersson, Carlos Xisto, Xin Zhao, Isak Jonsson, Anders Lundbladh, just to name a few, thank you for the excellent technical and non-technical discussions.

I would also like to send a lot of love to my fellow PhD student colleagues that I have had the pleasure of occupying the Turbo-room with, without you work would not be this fun. To my partner-in-crime Petter Miltén, whom I have worked with throughout Formula Student, master thesis and now PhD studies, I hope you are not tired of me. It has been and continues to be a privilege to call you my colleague and friend. To my friend and brother-from-another-department Carl Larsson, thank you for always improving my mood and for convincing me to pursue these studies. To my coach in all aspects of life, Adam Johansson, thank you for being a great friend and always being a beacon of positivity and source daily laughs. I am also really, really thankful of my friends outside of Chalmers for always believing in me. To all the people mentioned above – thank you.

And finally, I want to thank the most important people in my life, my loving and supportive family. Pappa Per, mamma Mi-Young, syster Josefin, svåger Martin, systerdotter Clara and farbror Ulf – this is for you.

Christian Svensson
Göteborg, November 2024

List of Publications

This thesis is based on the following appended papers:

Paper 1. Christian Svensson, Amir A.M. Oliveira and Tomas Grönstedt
Hydrogen fuel cell aircraft for the Nordic market

Paper 2. Christian Svensson, Petter Miltén, and Tomas Grönstedt
Modelling hydrogen fuel cell aircraft in SUAVE

Nomenclature

Acronyms

AoA	–	Angle-of-Attack
BoP	–	Balance-of-Plant
CFD	–	Computational Fluid Dynamics
CoG	–	Centre-of-Gravity
CO_2	–	Carbon dioxide
EDL	–	Electrical Double Layer
FC	–	Fuel Cell
GenHEX	–	Generalized Method for the Conceptual Design of Compact Heat Exchangers
GI	–	Gravimetric Index
HHV	–	Higher Heating Value
HT-PEMFC	–	High Temperature Proton-exchange Membrane Fuel Cell
LH_2	–	Liquid Hydrogen
LHV	–	Lower Heating Value
LT-PEMFC	–	High Temperature Proton-exchange Membrane Fuel Cell
MLI	–	Multi-Layer Insulation
MTOW	–	Maximum Take-off Weight
MZFW	–	Maximum Zero Fuel Weight
NACA	–	National Advisory Committee for Aeronautics
NASA	–	National Aeronautics and Space Administration
OEW	–	Operational Empty Weight
PAX	–	Passenger
PEMFC	–	Proton-exchange Membrane Fuel Cell
SAF	–	Sustainable Aviation Fuel
SL	–	Sea-level
SUAVE	–	Stanford University Aerospace Vehicle Environment
VLM	–	Vortex Lattice Method

Variables and parameters

A_{cell}	–	cell active area	–	[cm^2]
C_1	–	MLI model parameter	–	[-]
C_2	–	MLI model parameter	–	[-]
C_3	–	MLI model parameter	–	[-]
C_g	–	MLI model parameter	–	[-]
E	–	Young's modulus	–	[Pa]
E_h	–	Ideal reversible voltage	–	[V]
E_r	–	True reversible voltage	–	[V]
Δg	–	Gibb's free energy	–	[J/mole]
Δh	–	heat of reaction	–	[J/mole]
K	–	tank end-cap sphericity factor	–	[-]
L_{cyl}	–	length of cylindrical tank section	–	[m]
$N_{cells,stack}$	–	number of cells per stack	–	[-]
N_{stacks}	–	number of stacks in multi-stack	–	[-]
N_{MLI}	–	number of MLI layers	–	[-]
P	–	total system power	–	[W]
P_{BoP}	–	BoP power	–	[W]
P_{cell}	–	cell power	–	[W]
P_{prop}	–	useful propulsive power	–	[W]
P_{stack}	–	stack power	–	[W]
Pr	–	Prandtl-number	–	[-]
Q_{FC}	–	fuel cell system heat rate	–	[W]
Ra	–	Rayleigh-number	–	[-]
f_A	–	air utilization factor	–	[-]
i	–	current density	–	[A/cm^2]
k_{BoP}	–	BoP power overhead factor	–	[-]
$\dot{m}_{air,in}$	–	FC intake air mass flow	–	[kg/s]
$\dot{m}_{fuel}$	–	fuel mass flow	–	[kg/s]
m_{fuel}	–	fuel mass	–	[kg]
m_{tank}	–	tank mass	–	[kg]
n_g	–	MLI model parameter	–	[-]
p_{cell}	–	cell power density	–	[W/cm^2]
$p_{design,inner}$	–	design pressure inner tank wall	–	[Pa]
$p_{design,outer}$	–	design pressure inner tank wall	–	[Pa]
Δp_{inner}	–	pressure difference inner tank wall	–	[Pa]
Δp_{outer}	–	pressure difference inner tank wall	–	[Pa]
p_{MLI}	–	vacuum-jacket/MLI pressure	–	[Pa]
p_{max}	–	ventilation pressure	–	[Pa]
q_{MLI}	–	heat flux through MLI	–	[W/m^2]
r_1	–	inner radius inner tank wall	–	[m]
r_2	–	outer radius inner tank wall	–	[m]
r_3	–	inner radius outer tank wall	–	[m]
r_4	–	outer radius outer tank wall	–	[m]

t_{MLI}	–	thickness of MLI	–	[m]
$t_{w,inner}$	–	thickness inner tank wall	–	[m]
$t_{w,outer}$	–	thickness outer tank wall	–	[m]
T_C	–	MLI cold side temperature	–	[K]
T_H	–	MLI hot side temperature	–	[K]
V	–	system voltage	–	[V]
V_{cell}	–	cell voltage	–	[V]
η	–	system efficiency	–	[-]
η_{act}	–	activation loss	–	[V]
η_{conc}	–	concentration loss	–	[V]
η_i	–	ideal thermodynamic efficiency	–	[-]
η_{ohm}	–	ohmic loss	–	[V]
ϵ	–	emissivity	–	[-]
ν	–	Poisson's ratio	–	[-]
$\overline{Nu}$	–	Nusselt-number	–	[-]
σ_y	–	yield stress	–	[Pa]
e_w	–	weld weakness factor	–	[-]
SF_{inner}	–	safety factor inner tank wall	–	[-]
SF_{outer}	–	safety factor outer tank wall	–	[-]

Physical constants

F	–	Faraday's constant	–	96485 C/mole
N	–	number of electrons	–	2 mole
S_O	–	number of oxygen	–	0.5 mole
m_A	–	molecular weight dry air	–	$28.9655 \cdot 10^{-3}$ kg/mole
x_O	–	oxygen fraction dry air	–	0.2095

Contents

Part I

Introductory Chapters

Chapter 1

Introduction

1.1 Background

The commercial aviation industry is today a mainstay of modern life, with air transport enabling commerce, business and cultural exchange to occur at a truly global scale. To fully understand the scale of the business, it was estimated in 2019 that $876 billion was spent globally on air transport, with the airline industry employing 2.93 million people worldwide [1]. Since the introduction of commercial air travel in the 1950's, yearly passenger volumes have grown from a few million to roughly 4.5 billion in 2019 [2]. It is estimated that by 2050, this number will have more than doubled [3].

Commercial aviation was also responsible for 2.5% of global CO_2 emissions in 2019 [4]. This comes at a time when developments in engine, material and aerodynamic technology have made today's aircraft highly efficient in terms of fuel burn. For perspective, a state-of-the-art aircraft like the Airbus A320neo consumes roughly 77% less fuel per passenger compared to a Boeing 707 which was introduced in the dawn of the jet-era [5]. Small improvements are consistently introduced with each new turbofan or aircraft type, but the rate of improvement has slowed down as the technologies have reached a high level of maturity. The incremental efficiency gains coupled with the expected growth in passenger volumes makes for a situation incompatible with reaching net-zero global climate impact within the industry. To address this, alternative fuels and propulsion types are needed.

In the future, an airline's fleet is likely to use aircraft of different fuels and propulsion types. The medium to long haul market can be covered by turbofan aircraft either combusting hydrogen or Sustainable Aviation Fuel (SAF). These aircraft will be similar to the aircraft of today, with slight modifications to enable the use of the new fuels. For the longest haul flights, SAF is expected to be the viable alternative in the near future, as the hydrogen storage is relative heavy and very voluminous [5]. Aircraft with battery electric propulsion is an attractive option for short-haul flights, with its zero in-flight emissions, but due to limitations in current battery energy densities, it is limited to short-range flights under 230 NM [6]. The gap in-between the battery electric and hydrogen combustion aircraft can then be bridged by hydrogen fuel cell electric aircraft, which offers a better energy density

than the battery electric aircraft at a minimal climate impact. A proposed future airline fleet can be seen in Figure 1.1, where all of the above mentioned propulsion types are included.

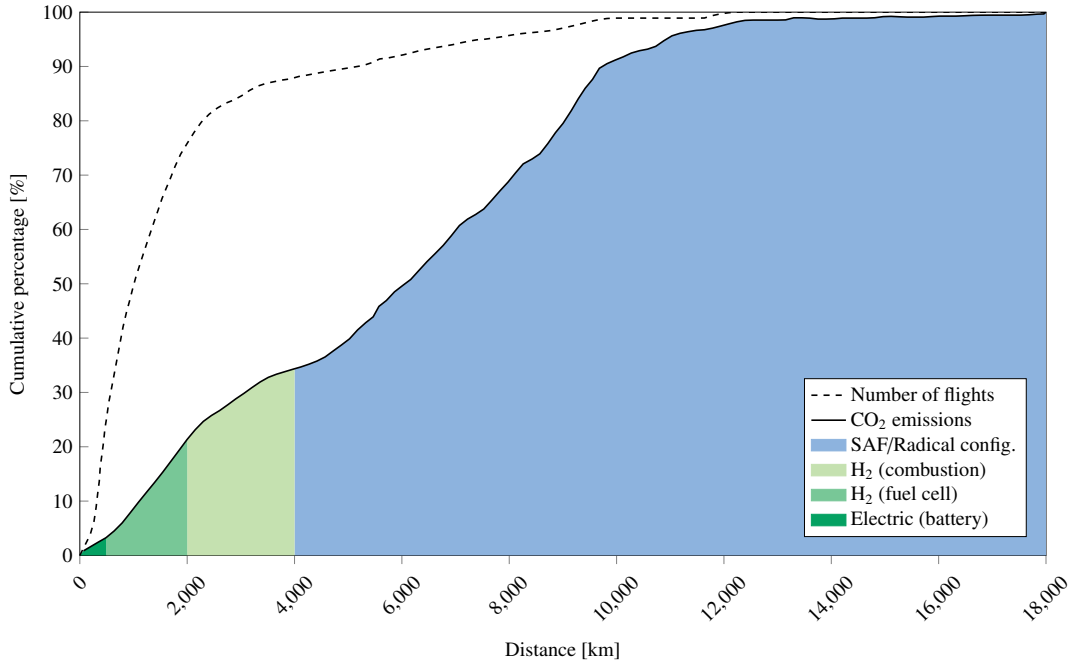

Figure 1.1: Proposed future share of propulsion types departing from a global airport. Cumulative line charts of CO_2 emissions and number of departing flights (data from Schiphol airport in 2018). Reproduced from [7].

1.2 Hydrogen in aviation

Research into hydrogen-fueled aircraft began more than half a century ago, and has been motivated by military, geopolitical and environmental aspects. One of the first research projects into hydrogen-powered flight was conducted by NACA (pre-cursor to NASA) in the 1950s. The military's desire to fly further, faster and higher demanded an alternative fuel with a greater heating value than the then standard JP-4 jet fuel. In a technical memorandum from 1955 on the subject of using liquid hydrogen (LH_2) for high-altitude aircraft [8], Silverstein and Hall hinted at one of the main success criteria for the introduction of hydrogen-powered flight:

"This increase in relative aircraft storage volume without sacrifice in aerodynamic efficiency provides the key to the successful exploitation of the high heating value per pound of the low-density liquid hydrogen.".

A cornerstone of hydrogen aircraft research is the collection of studies conducted by the Lockheed corporation during the oil-crisis in the 1970s. The research was compiled by Lockheed engineer Daniel G. Brewer into a classical text book on the subject [9]. In the research, two subsonic passenger transport aircraft were

conceptually designed – a 130 PAX short-range model, and a 400 PAX long-range model. In addition to the conceptual design of the aircraft at a full-system level, design concepts were proposed for sub-systems, such as the hydrogen tanks and refueling system. Both types were designed for a cruise Mach number of 0.85, and had the hydrogen storage both forward and aft of the fuselage. For the short-range aircraft, an increase of 3% was noted for the empty weight, but an 11% decrease in gross weight. This is common for hydrogen aircraft, where the fuel itself is light due to a better mass specific energy, but is penalized by the need of heavy insulated pressure vessels for containing the fuel (in contrast to storing conventional jet fuel inside the wings). Due to the extra volume needed for housing the hydrogen storage, wetted-area increased which caused an 18% drop in aerodynamic efficiency (lift-to-drag ratio) at cruise.

A more modern attempt at studying the technical feasibility of hydrogen transport aircraft is the European Union-funded Cryoplane project [10, 11], which was undertaken in the early 2000s. Similar to the work of Lockheed, a comprehensive study was made on aircraft concepts, fuel system design, safety aspects and economic feasibility. In terms of aircraft concepts, both conventional "minimum risk" (e.g. tube-and-wing planform) and unconventional (e.g. blended-wing-body planform) designs were explored. All aircraft sizes expected in a typical airline fleet were considered, including a small regional and a regional propeller aircraft. Interestingly the empty weight fraction (OEW/MTOW) was practically at a constant value of 0.68 for all types. The Maximum Take-off Weight (MTOW) per passenger nautical mile increased by 0.3% for the small regional and 4.4% for the regional propeller. The energy consumption per passenger nautical mile increased with 14% for both concepts. It was concluded in the project that while commercially operating a hydrogen aircraft was technically feasible, several obstacles remained, mainly economical. Hydrogen as an aviation fuel was deemed not economically competitive with conventional jet-fuel, and would instead require "some drastic political event or action" in order to bring on transition.

It is seen in general that the energy consumption for hydrogen aircraft is expected to be higher than that of their kerosene counterparts, mainly due to increased wetted area and weight, both contributing to increased aerodynamic drag. Here, it should be noted that for advanced tank technology, hydrogen aircraft may actually get lighter at take-off, despite their generally higher energy need. This is due to the much higher energy content per kg for hydrogen [12] as compared to its Jet A counterpart. The generally observed higher energy need makes the case for transitioning to hydrogen challenging, as 2020 estimates put LH_2 at 4-6 times the price per energy content of kerosene in Europe [13]. Furthermore, it is expected that there will be a large disparity of LH_2 prices between small and large airports in the future, with year 2050 projections estimating LH_2 being 110% more expensive than kerosene at small airports and 56% at large airports [14]. If no major technical leaps are made, either by large improvements to existing designs, or by radically altering the state-of-the-art [15], the energy consumed by this type of aircraft will be increased. If changing the airframe layout radically is deemed too high of a risk, an option could be to switch to electric propulsion. As batteries suffer from extremely low energy densities,

fuel cell based electric propulsion becomes the most attractive option.

1.3 Fuel cell aircraft

Fuel cell propulsion using LH_2 is a promising option for reducing the climate impact of aviation in the regional segment. This market segment represents a substantial portion of the global fleet emissions, with estimates putting flights under 2000 km responsible for a third of CO_2 emissions [16]. This is a result of the large amount of flights made within this segment, and that regional aircraft's CO_2 intensity (kg of CO_2 per passenger kilometer) is estimated to be 80% higher when compared to narrow and wide body aircraft [16]. A reason for this difference in CO_2 intensity is thought to be due to more research efforts going into larger aircraft, e.g. turbofan single-aisle types. It is therefore motivated to use hydrogen fuel cells within regional class flights, many of which are served by turboprop aircraft such as the ATR 42, ATR 72 and Dash-8. As current proton-exchange membrane fuel cell (PEMFC) propulsion systems are in the range of 1.5 kW/kg at a system level [17], the system is relatively heavy when comparing to turbine-based powerplants such as a turboprop engine (PW127 family of engines' specific power is around 4 kW/kg [18]). The promising aspect of fuel cell systems is then its much greater system efficiency, which for larger systems are in the order of 45-60% [19] compared to a conventional turboprop's range of 20-30% [19].

In the case of a powering a regional turboprop aircraft on hydrogen fuel cells, such as an ATR 42, the turboprop engine is replaced with an electric motor, which rotates the propeller. The needed electrical power is produced by running a fuel cell system, which uses gaseous hydrogen and oxygen in its reaction to produce electricity. The oxygen is extracted from the freestream air, while the hydrogen is stored on-board in tanks.

A single fuel cell is not enough for most applications, especially aircraft which need useful power outputs in the order of megawatts. Therefore multiple fuel cells are connected in series into so-called stacks. In addition to the actual fuel cells, the system has auxiliary systems which are needed to sustain the process, and are referred to as Balance-of-Plant (BoP) components. They are responsible for air supply, hydrogen supply, heat rejection among other things which all help to sustain the electro-chemical process. A more detailed walk-through of the fuel cell propulsive system is made in Chapter 2.

The hydrogen is most commonly stored cryogenically to maximize the gravimetric density and require insulated pressure vessels to have allowance for boil-off-induced pressure rise. It is then pumped and heated in order to enter the fuel cell in a gaseous phase at the right temperature and pressure. The tanks are usually filled at pressures slightly higher than sea-level, and will permit a maximum internal pressure of around 2-5 bar. More details on tank design and hydrogen boil-off mitigation is detailed in Chapter 3.

The lowest risk option for integrating hydrogen fuel cell propulsion into regional aircraft is to perform a retrofit, whereby an existing airframe is fitted with new nacelles, housing an electrical motor and fuel cell system, and accommodating the

hydrogen tanks inside the fuselage. For a regional aircraft the tanks can be placed in the aft of the fuselage, as the fuel mass is in the order of a few percent of the total weight, and therefore does not cause excessive in-flight shift of the centre-of-gravity (CoG) (see Paper 2). As the tanks take up significant volume, the seating capacity of an retrofit is reduced in order to accommodate this. Another option is to perform a redesign, where you build a new airframe based on an existing design. This could involve stretching the fuselage in order to accommodate the tanks without sacrificing the cabin size.

1.3.1 Demonstrator flights

There have been several manned flights using fuel cell propulsion, both from small and larger regional-sized aircraft. In 2008 Boeing successfully flew a converted Diamond HK36 Super Dimona two-seat motor-glider to a cruising altitude of roughly 1000 m above sea-level using a battery-fuel cell hybrid system [20]. Once at cruising altitude, the batteries were disconnected and power was then solely provided by the PEMFC system. The original MTOW was 770 kg, which was increased with 100 kg after the propulsion system swap. The PEMFC system had a gross maximum power output of 24 kW, and was fed with hydrogen from a 350 bar high-pressure tank.

In 2016 the German Aerospace Center (DLR) performed the maiden flight of the HY4 aircraft [21]. It is a four-seat aircraft, consisting of two fuselages, with the nacelle and propulsion system located in-between. The single electrical motor had a maximum power output of 80 kW, which was like Boeing's demonstrator powered by a battery-fuel cell power source. In 2023 the gaseous high-pressure hydrogen storage was switched out and successfully flew using liquid hydrogen storage [22].

For regional-sized demonstrators there have been flights made by two hydrogen aircraft manufacturers. In 2023 Universal Hydrogen completed ts first flight of a fuel cell converted Dash 8-300, where one of the two turboprops was switched out for a fuel cell propulsion system [23]. The company is now defunct, but was in the midst of developing conversion kits for the Dash-8 and ATR 72 aircraft. This involved a modular liquid hydrogen tanks, not dissimilar from cargo containers already in use in aircraft. The company also was able to test a megawatt-level fuel cell propulsion system in a ground test-rig in 2024 [24].

ZeroAvia is a company developing fuel cell propulsion systems and has performed several flights with a 19 passenger Dornier 228 [25], with the maiden flight in 2023. One of the turboprops was swapped for the company's 600 kW ZA-600 powertrain [26]. The company is also developing the 2-5 MW ZA-2000 powertrain [19], intended for regional turboprop-style aircraft in the 40 to 80 passenger range.

Chapter 2

Fuel cell propulsion

2.1 Operating principle

A fuel cell is a electrochemical device which is able to convert chemically stored energy into electrical energy. A modern PEMFC system does this by feeding gaseous hydrogen into the anode section of the cell, where a catalyst causes the hydrogen to split into a positively charged ion (proton) and a free electron. The proton is then able to pass through a membrane to the cathode side. The free electron is forced to travel through an electric circuit to the cathode side, at which the positively charged hydrogen, oxygen (usually from air) and free electron combine to form water, as seen in Equation 2.1.

$$\mathrm{H_2} + \frac{1}{2}\,\mathrm{O_2} \longrightarrow \mathrm{H_2O} + \text{heat} \tag{2.1}$$

The water-forming reaction is exothermic, and therefore energy is released. This heat of reaction amounts to the enthalpy difference between forming the products and reactants. Using the higher-heating-value (HHV) of hydrogen, which is the correct caloric value when considering a low-temperature PEMFC (LT-PEMFC), the heat of reaction released in Equation 2.1 for a 80°C PEMFC amounts to $-\Delta\ h =$ 286 kJ/mole [27]. The ideal reversible voltage E_h is found using Nernst's relation,

$$E_h = -\frac{\Delta h}{N \cdot F} \tag{2.2}$$

where F is Faraday's constant and N the number of electrons released by the anode half-reaction. At 80°C E_h corresponds to 1.472 V [27].

Due to losses it is not possible to convert the entirety of the energy released into useful work. By subtracting the losses due to entropy generation, we get Gibbs free energy Δg, which is then a measure of the theoretical maximum energy which can be extracted from the reaction. Using Nernst's equation again, the true reversible cell voltage becomes,

$$E_r = -\frac{\Delta g}{N \cdot F} \tag{2.3}$$

which corresponds to 1.180 V at 80°C [27]. The ideal thermodynamic efficiency can then be calculated as

$$\eta_i = \frac{E_r}{E_h} = \frac{1.180}{1.472} = 0.8 = 80\% \quad . \tag{2.4}$$

In reality this is not achievable, due to losses in the reaction and transport of current.

2.1.1 Cell characteristics

A fuel cell chemistry can be characterized by its voltage V_{cell} [V] as a function of the input current density i [A/cm^2]. This is known as the fuel cell's polarization curve, and is used for defining the cell's efficiency η_{cell} and power density p_{cell} [W/cm^2], as well as for sizing the active area A_{cell} [cm^2] to achieve the wanted stack-level performance. Figure 2.1 illustrates a modern LT-PEMFC chemistry [27].

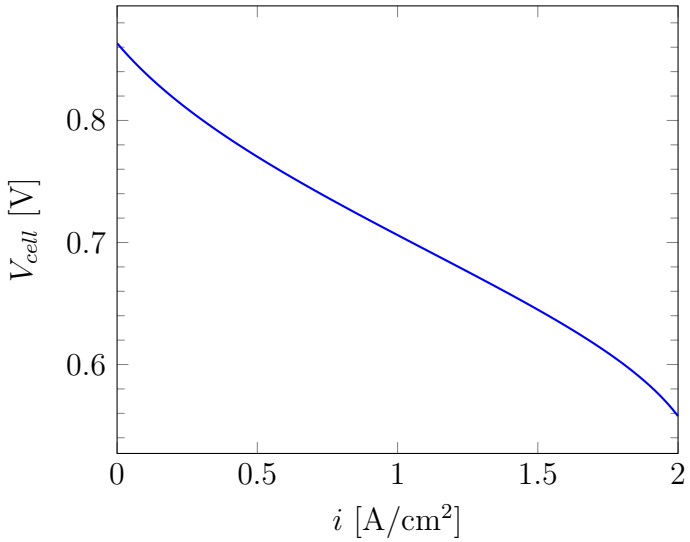

Figure 2.1: Cell voltage as a function of input current density. Modern PEMFC operating at 2.5 bar [27].

As seen in Figure 2.1, the actual cell voltage is the true reversible cell voltage minus three losses

$$V_{cell} = E_r - \eta_{act} - \eta_{ohm} - \eta_{conc} \quad . \tag{2.5}$$

The activation loss (η_{act}) relates to the overpotential needed in order to overcome the activation energy, which is the energy needed for the charged particle to pass through the electrical double layer (EDL) (a layer of varying charge) at the electrode surface. The loss is prominent at low currents, as a large portion of the particle's energy will go into overcoming this energy, which as a result slows down the rate of reaction. At higher current the loss is practically linear, with it slowly increasing with current.

The ohmic losses (η_{ohm}) are due to resistance in the electron and ion transport, which occur in the electrodes and the circuit connecting them. As it follows Ohm's law, it is directly proportional to the input current.

The concentration losses (η_{conc}) are caused by an imbalance between the the consumption and supply of the fuel/oxidizer at the electrode. The loss increases quickly at higher currents and will determine the point of highest possible current.

With the voltage-current density relation defined, the power density can be characterized. As is seen in Figure 2.2, there is an maxima to the power density curve. As it is the power produced per active cell area, sizing the fuel cell system so that the maximum power coincides with this point will yield the smallest required cell area, and therefore lightest possible fuel cell stack.

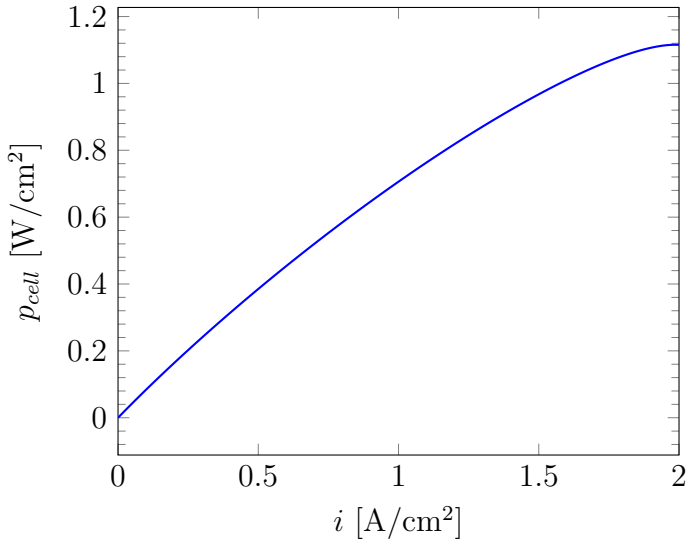

Figure 2.2: Power density as a function of input current density. Modern PEMFC operating at 2.5 bar [27].

As was mentioned in the previous section, the theoretical thermodynamic efficiency of the fuel cell was 80%. With the real losses defined, the true cell efficiency can be defined as

$$\eta_{cell} = \frac{V_{cell}}{E_h} \quad . \tag{2.6}$$

When plotting the cell efficiency for the range of input current densities, as seen in Figure 2.3, it is clearly observed that a fuel cell will deliver power most efficiently at lower loads. In order to maximize the efficiency during operation, the stack should then be sized for higher power levels than what is actually required during operation, so that the operating point for peak power occurs at the fuel cell's most efficient.

It is clear from the polarization curve that there are many ways to size the fuel cell system. Sizing for max power density will yield the lowest overall area and therefore mass and volume, but is on the other hand not in the most efficient range. Sizing for lower input currents will yield a more efficient system, but requires the system to be over-dimensioned, which carries a mass and volume penalty.

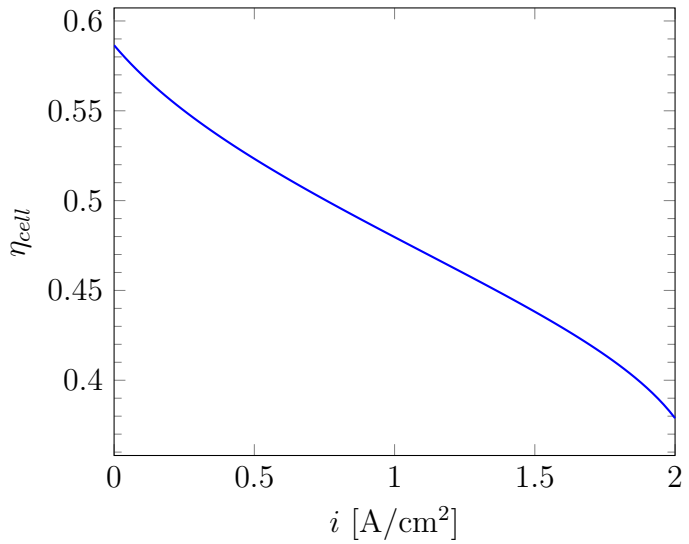

Figure 2.3: Cell efficiency as a function of input current density. Modern PEMFC operating at 2.5 bar [27].

2.2 Multi-stack design

In order to develop an appropriate system voltage, multiple fuel cells have to be connected in series. The number of cells per stack is then directly related to the system voltage,

$$V = N_{cells,stack} V_{cell} \tag{2.7}$$

where $N_{cells,stack}$ is the number of cells in a stack. This solves the voltage part of the sizing, but might not deliver enough power for the given application. By connecting multiple of these stacks in parallel, we maintain the voltage set by one stack, but get the combined power of all stacks. The power produced by one fuel cell (P_{cell} [W]) is determined by the power density and active area

$$P_{cell} = p_{cell} A_{cell} = (i V_{cell})\, A_{cell} \quad . \tag{2.8}$$

The total power produced by a single stack is then,

$$P_{stack} = N_{cells,stack} P_{cell} \tag{2.9}$$

and the total system power

$$P = N_{stacks} P_{stack} \tag{2.10}$$

where N_{stacks} are the number of stacks connected in parallel in multi-stack configuration.

It is now possible for a given sizing point ($[i_D, V_{cell,D}]$), desired maximum total system power (P_D) and voltage (V_D) to size the multi-stack. A principal illustration of a multi-stack (without the BoP) is shown in Figure 2.4. The length of the stack is naturally dictated by the total effective thickness of one fuel cell, but is also very much controlled by the design choice of cell's and total system voltage at the design

point. The width and height of a single stack roughly follow the active area of the cells, which can be controlled with varying the amount of stacks in the multi-stack.

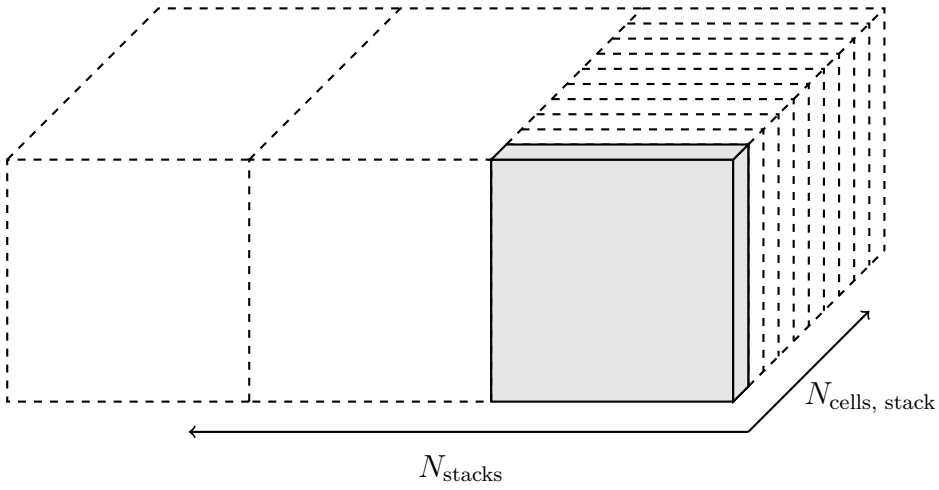

Figure 2.4: Illustration of multi-stack configuration.

2.3 Balance-of-Plant

The balance-of-plant includes any component which is essential in sustaining the fuel cell's operation. The components can be grouped into systems such as the fuel supply, air supply, thermal management, water management and power control. Some of these systems are parasitic power losses, such as the air compressor, while a turbine in the fuel cell system's exhaust can recover some small amounts of power. Other systems such as the fuel storage are passive or at least do not consume any significant amounts of power. Nevertheless, the BoP causes extra drag to the aircraft as it takes up volume and adds weight to the system. Some components such as the heat-exchanger for the cooling system can cause significant increases in drag as it interacts with a large area of incoming air and will itself cause loss of total pressure thereby momentum drag.

The total power produced by the fuel cell multi-stack has to provide both the propulsive power needed for the electric motor as well as the power drawn by the BoP. The total power produced by the fuel cell system is then

$$P = P_{prop} + P_{BoP} = k_{BoP} P_{prop} \quad . \tag{2.11}$$

The BoP's share of the total system varies with the thrust and ambient conditions. Furthermore, the a BoP component's share of the total BoP power will also vary. As an example, take-off in a warm climate will require large amounts of heat rejection due to high propulsive power, which is made difficult by the low dynamic pressure and high ambient temperature. This is the operating point for which the cooling will draw maximum power. But due to the ambient static pressure on-ground, the compressor will not work at full capacity to boost the inlet pressure to the needed

fuel cell stack pressure. Conversely, in cruise conditions the total pressure is roughly half of that at beginning of take-off, which requires more compressor power. But at this altitude there might be an ambient temperature 60 to 70 degrees lower than that of a hot-takeoff, which strains the cooling system much less. It is difficult to get around the need of active air compression due to the ambient air density decreasing with increased altitude. On the topic of cooling there are several things that can be done to remedy the problem. One of them is to switch to high-temperature PEMFCs (HT-PEMFC), which increases the operating temperature and thereby also increases the temperature difference to the ambient. This in hand will decrease the required heat-exchanger size.

The total system efficiency can then be defined using k_{BoP} and the cell efficiency previosuly defined in Equation 2.6

$$\eta = \frac{\eta_{cell}}{k_{BoP}} = \frac{P_{prop}}{P}\eta_{cell} \quad . \tag{2.12}$$

2.4 Reactant usage and heat produced

In order to evaluate the mission performance of a fuel cell aircraft, the resulting fuel mass flow has to be calculated. With the efficiency and power output known of the fuel cell system, the mass flow is calculated according to

$$\dot{m}_{fuel} = \frac{P}{HHV \cdot \eta_{cell}} = \frac{P_{prop}}{HHV \cdot \eta} \quad . \tag{2.13}$$

The mass flow of air needed to supply the required oxygen for the cathode half-reaction is dictated by [27],

$$\dot{m}_{air,in} = f_A \left(\frac{S_O m_A}{x_O N F} \right) \frac{P}{V_{cell}} \tag{2.14}$$

where f_A is the utilization factor, where values larger than one indicate supply is greater than consumption (usually 1.5-2.5 for typical systems [27]). S_O is the moles of oxygen, N the moles of electrons, F Faraday's constant, m_A the molecular weight of air and x_O the fraction of oxygen in air. P is the total power output of the system and V_{cell} the cell voltage. Although air is quite readily available for an aircraft and therefore not as finite as the on-board hydrogen, the needed mass flow of air is important to know for designing and evaluating the performance of the air intake system.

The rate of waste heat produced by the system is simply the potential power of the reaction not converted into usable electric power

$$Q_{FC} = \left(\frac{1}{\eta_{cell}} - 1 \right) P = \left(\frac{1}{\eta} - 1 \right) P_{prop} \quad . \tag{2.15}$$

Some of this heat is rejected via the air exhaust and through being absorbed by the structure and convected away, but the majority of this heat has to be rejected via the dedicated liquid-air cooling system.

Chapter 3

Hydrogen storage

3.1 Fuel characteristics

Hydrogen offers the highest caloric value out of any available fuel. The lower heating value (LHV) is at 120 MJ/kg [28], which is roughly three times larger than conventional Jet-A (43 MJ/kg [28]). This makes hydrogen an attractive fuel for many transport applications, especially within rocketry and aviation as overall vehicle mass plays a big role in the vehicle's performance. Hydrogen has successfully been used in experimental aircraft (see Chapter 1), but has seen most use within orbital launch systems, such as in NASA's Space Shuttle main engines.

As was described in Chapter 1, the main challenge with hydrogen is its low volumetric mass density. At 1 bar and 20°C the density of hydrogen is 0.084 kg/m^3 [29], which despite its great LHV causes infeasible storage volumes when comparing to the density of Jet-A which is around 804 kg/m^3. To get around this problem, hydrogen used in cars and trucks is usually pressurized to either 350 bar, at which the density is approximately 24 kg/m^3 [29], or to 700 bar where the density is 40 kg/m^3 [29] (both at 20°C). This would still yield infeasible storage volumes for an aircraft. To put things into perspective, an ATR 42 turboprop has a maximum fuel capacity of 4500 kg, which in terms of volume and energy content is roughly 5.6 m^3 and 193 GJ when considering Jet-A. For the same energy stored, hydrogen would bring down the fuel mass to 1608 kg. But the benefits in mass are quickly diminished by the new required storage volume. The volume for storing this amount of hydrogen at 700 bar would end up being 40 m^3, or seven times the volume when compared to the original Jet-A aircraft! For this volume to fit inside the fuselage width of 2.58 m, the resulting cylinder of pressurized hydrogen would be 7.7 m, which is a majority of the existing cabin length. In addition, high-pressure tanks are notoriously heavy, with the fuel mass in many cases only constituting 5% of the combined fuel and tank mass, meaning the system itself would be heavier than the ATR 42 take-off mass.

By cooling down the hydrogen gas to around -253°C (at SL pressure), we can achieve liquefaction. This bumps up the density to 71 kg/m^3 [29], which starts becoming more acceptable for integration into aircraft. For the previous example of the ATR 42 with pressurized hydrogen at 700 bar, the use of liquid hydrogen

would reduce the required cylindrical storage volume to roughly 22 m^3, a three meter decrease in occupied fuselage length.

The challenge with liquid hydrogen is the process of the liquid starting to boil and subsequently vaporizing into hydrogen gas, creating so called boil-off. With the hydrogen's state located on the saturation curve, any heat added to the liquid will cause it to start boiling. This will raise the pressure inside the tank. If the pressure increases to the design limits of the pressure vessel, action has to be taken. The gas can then either be ventilated through a valve to atmosphere. If the boil-off is not reliquified or used in some other way, this will constitute a loss of usable fuel. Boil-off is inevitable, and therefore care has to be taken to limit its rate. This is primarily done with effective thermal insulation and with powered devices which can mix the fuel and prevent thermal stratification.

3.2 Cryogenic storage

Liquid hydrogen presents unique challenges for the storage system in terms of its ability to withstand heat transfer from the environment, internal and external pressure loading, as well as hydrogen related peculiarities such as tank wall embrittlement and permeability.

While the pressure at which the LH_2 is filled at (fill pressure) is usually only slightly above SL, which is done in order to minimize risk of air entering in case of catastrophic tank failure, the tank has to be designed to withstand the internal pressure created by the boil-off and the external pressure by the ambient atmosphere outside the tank. If the boil-off progresses until the pressure inside the tank is at the design's rated limit, the gas has to be vented out of the tank. This outflow of enthalpy reduces the internal energy of the tank contents, and therefore reduces the pressure and temperature. The pressure at which ventilation is triggered (ventilation pressure) is one of the key design parameters for the tank's overall performance, as it determines the wall thickness, which affects the weight and the overall ventilated mass throughout a mission.

When filling the tank, a certain amount of gas will be put in the tank in order to be able to reduce the pressure if the tank reaches the ventilation pressure at maximum fuel load. This is known within cryogenic storage as gas ullage, and common levels are 3% [30]. This means that when the tank is filled to its maximum, the fuel can pressurize up to the ventilation pressure, and still have 3% of its volume to be occupied by gas that can be ventilated in order reduce the pressure. This is needed as a safety precaution, but also has performance implications. If considering two tanks with the same fill pressure and desired gas ullage, a tank with higher ventilation pressure will have to have a higher initial fraction of gas, in other words less fuel mass. Figure 3.1 illustrates this behavior for tanks identical in all aspects except ventilation pressure.

As the fuel tank has to have minimal surface area, be able to resist pressure, and not leak, the hydrogen has to be contained in dedicated insulated pressure vessels. Compared to conventional aircraft which generally stores the kerosene inside tanks integral to the wings, the main performance concern for hydrogen storage becomes

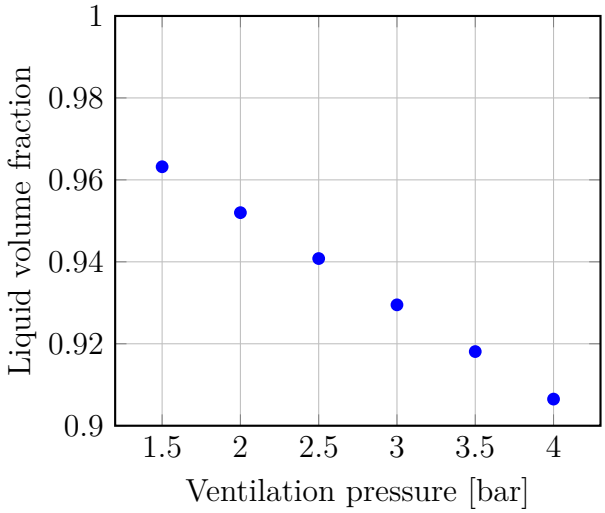

Figure 3.1: Effect on liquid volume fraction $\left(\frac{V_{LH_2}}{V_{LH_2}+V_{GH_2}}\right)$ by changing the ventilation pressure.

its weight and the volume it occupies. A tank's mass efficiency in storing the fuel is commonly classified by gravimetric index (GI), which is defined as the ratio between the fuel's mass and the combined mass of the fuel and tank

$$GI = \frac{m_{fuel}}{m_{fuel} + m_{tank}} \quad . \tag{3.1}$$

A conventional Jet-A aircraft with integral wing tanks will have a GI of 100%. The reported numbers of GI for LH_2 tanks from both theoretical models and real-world prototypes have a large spread. Depending on pressure vessel design, which entails shape, material and pressure limits, and the type and amount of insulation, GI can range between 15% to as high as 90% [31]. The Clean Sky 2 project assumed 30% for their regional fuel cell aircraft, with GI's going up to 37-38% for the medium and long range concepts [13]. Verstraete [32] estimated the GI for a single regional aircraft tank to be between 67.5-70.9% depending on chosen insulation type.

A key question is what GI has to be achieved in order to reach parity with conventional Jet-A aircraft in terms of energy consumption. In [31] it is shown that a GI of around 55% is needed in order for a regional aircraft to reach similar energy consumption levels as its conventional counterpart (if only difference in fuel and tank weight is considered).

3.2.1 Insulation system

An effective insulation system is needed to limit the amount of heat being transferred from the ambient environment to the fuel. The external surface of the tank will be affected by convection and radiation from the environment, which depending on the type of insulation, will conduct and radiate heat to the solid tank wall, which finally conducts the heat to the fuel. The thermal radiation absorbed by the tank is minimized by using low emissivity coating or paint. The external convection is

minimized by reducing the amount of movement of air outside the tank, and is in the case of internal non-integral tanks (such as an aft-mounted tank behind the aft pressure bulkhead) mostly limited to natural convection. The conductivity is minimized by covering the pressure vessel with a material of low thermal conductivity, such as low-density foam.

The most common types of insulation that are considered for aircraft are either foam-based or multi-layer insulation (MLI) systems. The two alternatives are effective solutions, but perform differently in terms of complexity, cost, density, thickness and overall thermal resistance. The foams are cheaper and less complex than the MLI, but have orders of magnitude higher thermal conductance. Common types are either polyurethane or polymethacrylimide (such as Rohacell®). These foams come in different densities, with polyurethane having densities of 32-64 kg/m^3 and thermal conductivity is in the order of 10^{-4}-10^{-2} W/m·K [33]. The MLI performs much better in this regard, with thermal conductivities in the order of 10^{-8}-10^{-5} W/m·K [33].

The foams are simple in that the only extra essential component involved is a vapor-barrier to prevent water condensation from being absorbed into the material, which would reduce its effectiveness. The MLI systems are considerably more complex and delicate. MLI consists of multiple thin radiation shields (like Mylar®), separated by a low-conductivity spacer material, all housed in a near-vacuum (usually in the order of one millibar). In a vacuum, similar to in space, the only means of heat transfer is radiation. But if the radiation shields would be in contact with each other the heat could conduct through the layers, hence the spacer-material. The main drawback of the MLI system is the vacuum, which has to be contained in a vacuum-jacket. This requires an extra outer tank wall, which adds weight.

The work covered in this thesis has only considered MLI tanks, as it is more effective in preventing heat transfer and takes less space. This simplifies the integration of the tanks into typical turboprop fuselage geometries.

A simple model of a tank subjected to heat transfer from the environment is illustrated in Figure 3.2. If the liquid-gas mixture is considered homogeneous in terms of pressure and temperature, the mechanisms involved in the heat transfer are

- External convection (ambient air) and radiation on external surface
- Conduction through insulation and tank wall
- Internal convection (fuel) on internal surface

For the work considered in this thesis, the external and internal convection heat fluxes are solved for by using Nusselt-number correlations for natural convection occurring along a vertical plate, where the length is set as the tank diameter [34]. The external convection considers ambient air, and internally the calculation is done separately for the liquid and gaseous volumes

$$\overline{Nu} = \left[0.825 + \frac{0.387 Ra^{1/6}}{(1 + (0.492/Pr)^{9/16})^{8/27}}\right]^2 \quad . \tag{3.2}$$

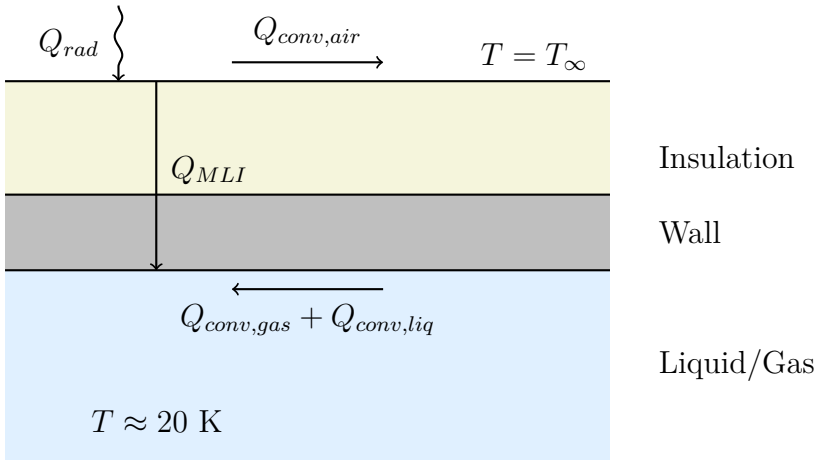

Figure 3.2: Illustration of heat transfer occurring between the liquid-gas fuel mixture, the tank wall, insulation and the ambient.

The metal tank wall is considered to not provide any thermal resistance, and it is then only the MLI system providing it. The flux through the MLI can be evaluated in bulk using an adaptation [35] of the semi-empirical Lockheed model [36],

$$q_{MLI} = C_1 N_t^{C_2} \frac{(T_H + T_C)(T_H - T_C)}{2(N_{MLI} + 1)} + C_3 \epsilon \frac{T_H^{4.67} - T_C^{4.67}}{N_{MLI}} + C_g \frac{p_{MLI}}{N_{MLI}} (T_H^{n_g} - T_C^{n_g}) \tag{3.3}$$

where T_H and T_C are the hot and cold surface temperatures, respectively.

The total heat transfer rate into the tank is then calculated by solving for Q_{MLI}

$$\begin{aligned} Q_{conv,air} + Q_{rad} &= Q_{MLI} \\ Q_{conv,gas} + Q_{conv,liq} &= Q_{MLI} \quad . \end{aligned} \tag{3.4}$$

3.2.2 Pressure vessel design

Cryogenic tanks can be classified into different types, with the difference being the type of material used in the pressure vessel.

Type 1 covers basic metallic tanks, made out of steel or aluminium alloys. Aluminium is a common choice in cryogenics due to stable mechanical properties when cooled, with alloys 2219 and 5083 being common for pressure vessels. This type of tank is considered in the work covered by this thesis, as it is a low-risk option technology wise and can easily be designed in conceptual aircraft studies with simple calculations.

Type 2 is a mix between metal and composites. An inner liner of metal is used to contain the hydrogen, due to being less permeable than composites. A fiber-reinforcement such as carbon fiber is then wrapped around the metal liner in order to absorb the hoop stresses. This decreases the weight of the system, without fully depending on a composite laminate for containment.

Type 3 is an evolution of the Type 2 with more fibers in more load paths. With the composite part also absorbing longitudinal stress in addition to the hoop stresses, the mass of the metal inner layer is further reduced.

Type 4 is a fully wrapped composite tank with a non-metal inner layer, usually a polymer-based liner. This gives a very light design, but increases the risk of hydrogen permeation.

Type 5 is a liner-less tank made solely out of composites, with the laminate structure both containing the hydrogen and taking up mechanical load. Although the lightest out of the different types, further research and testing is still needed to prove safe functionality.

Regardless of tank type, the fundamental load case for cryogenic tanks in aircraft is the same. The liquid-gaseous hydrogen mix is stored at slightly elevated pressures, which causes internal pressure load on the vessel. The maximum load considered is the ventilation pressure p_{max}. For an MLI tank which consists of a double pressure vessel, the inner wall experiences an effective pressure of,

$$\Delta p_{inner} = p_{max} - p_{MLI} \tag{3.5}$$

where p_{MLI} is the pressure between the outer and inner tank walls. A factor of 1.1 is added to account for ventilation valve defects, and a factor of two for in-flight dynamic loads, yielding a design pressure of

$$p_{design,inner} = 2 \cdot (1.1 \Delta p_{inner}) \quad . \tag{3.6}$$

The outer wall is subjected to external pressure loading, as its external surface is at ambient pressures, with the inside being the partial vacuum. The highest pressure experienced by the outer wall will be SL pressure,

$$\Delta p_{outer} = p_{\infty,max} - p_{MLI} \tag{3.7}$$

where $p_{\infty,max}$ is the pressure experienced at SL. Accounting for dynamic loads, the design pressure for the outer shell becomes

$$p_{design,inner} = 2 \cdot \Delta p_{inner} \quad . \tag{3.8}$$

With the design pressures known, the wall thickness of each shell can be calculated using formulas for pressure vessels. The inner thickness is solved for by considering welded metallic pressure vessels [37],

$$t_{w,inner} = r_2 - r_1 = \begin{cases} \frac{2 \cdot p_{design,inner} \cdot r_2 \cdot K}{2 \cdot (\sigma_y / SF_{inner}) \cdot e_w - 2 \cdot p_{design,inner} \cdot (K - 0.1)} & \text{(spherical)} \\ \frac{2 \cdot p_{design,inner} \cdot r_2}{2 \cdot (\sigma_y / SF_{inner}) \cdot e_w - 0.8 \cdot p_{design,inner}} & \text{(cylindrical)} \end{cases} \tag{3.9}$$

where the factor K is the sphericity of the endcaps, e_w a welding weakness factor and SF_{inner} the safety factor put on the yield stress. As is seen in Equation 3.9, there are two cases: purely spherical or cylindrical. In the case of non-spherical tanks, a cylinder with hemispherical endcaps is considered. In this case separate calculations are made using both cases, where the largest wall thickness of the two is set as the common wall thickness. The outer shell is loaded inwards, and therefore has to cope

with buckling loads. Therefore the wall thickness is solved for by using equations for curved panel buckling [38],

$$t_{w,outer} = r_4 - r_3 = \begin{cases} \sqrt{\frac{p_{design,outer} \cdot SF_{outer} \cdot r_4^2}{0.365E}} & \text{(spherical)} \\ \left[\frac{\left(p_{design,outer} \cdot SF_{outer} \cdot L_{cyl} \cdot r_4^3/(0.807E)\right)^4}{(1/(1-\nu^2))^3} \right]^{1/10} & \text{(cylindrical)} \end{cases} \tag{3.10}$$

where $r_3 = r_2 + t_{MLI}$, L_{cyl} the length of the cylindrical section and SF_{outer} the safety factor on the critical buckling pressure.

Chapter 4

Aircraft sizing and simulation

4.1 SUAVE

In order to evaluate the performance of fuel cell aircraft, methods for sizing and simulating the aircraft and its systems are needed. For this purpose, the open-source aircraft conceptual design tool Stanford University Aerospace Vehicle Environment (SUAVE) [39] is used. The software is comprehensive in its ability to build and analyze both conventional and unconventional designs [40]. To begin designing, the aircraft is fully parametrized in terms of airframe and propulsive systems, and can then be run through analysis methods such as classical text-book weight correlation methods, e.g. [41], and aerodynamic mapping through the built-in Vortex Lattice Method (VLM) solver [40]. With the aircraft fully defined, it can then be ran through the mission solver, which simulates flying a mission and will produce results such as total fuel burn.

4.2 Aircraft sizing

When designing the aircraft and its systems, more often than not sizing routines are incorporated in order to automate and ensure consistency in the aircraft's design. For the purposes of the work covered in this thesis, the aircraft sizing involves routines for:

1. Fuel cell system sizing
2. Cryogenic storage sizing
3. Airframe re-sizing

In the fuel cell system sizing the full multi-stack is designed together with the BoP components. The important input parameters involved here are the required maximum propulsive power, the maximum system voltage and wanted stack-up of the stacks inside the multi-stack. Given these inputs and a sizing point on a fuel cell polarization curve, the resulting BoP overhead (and by that total system power), mass and volume is calculated.

The routine for designing the MLI pressure vessels will output a resulting mass and volume, which depending on the design strategy might require a stretch of the baseline fuselage design. By giving the wanted number of tanks, maximum allowed radius, fill pressure, gas ullage and ventilation pressure, most parameters for the mechanical design are set. What is not as easy to define is the total fuel volume and thickness and density of the MLI system. An initial guess is made, which is then evaluated through mission solving. After this it can be evaluated if the amount of unused fuel, boil-off and ventilation behavior are deemed acceptable. Some tanks will make the overall aircraft performance worse than others, but there will also be a set of parameter combinations which results in excessive ventilation or pressures dropping below the fill-pressure safety limit. In most cases when evaluating tank performance a parameter sweep study is set up, which results in a feasible design space for the tanks.

Resizing the airframe in the case of the work covered here consists of modifying a baseline turboprop aircraft to accommodate the new propulsion system. If passenger capacity is to remain unchanged, a stretch or diameter increase of the existing fuselage has to occur. This increases the weight of the fuselage, translates the empennage rearward, and will have an impact on the overall aircraft CoG. If maintaining performance and airport compatibility of the baseline aircraft is desired, certain sizing rules have to be enforced, such as maintaining the baseline aircraft's wingloading and power-to-weight ratio. With this, any increase in aircraft weight will have to be compensated with larger wing area and increased propulsive power, both of which increase the aircraft weight. The resizing is therefore an iterative process, which is considered complete when the aircraft weight and CoG are converged. The iterative re-sizing is illustrated in Figure 4.1, and an example of resized ATR 42 is shown in Figure 4.2.

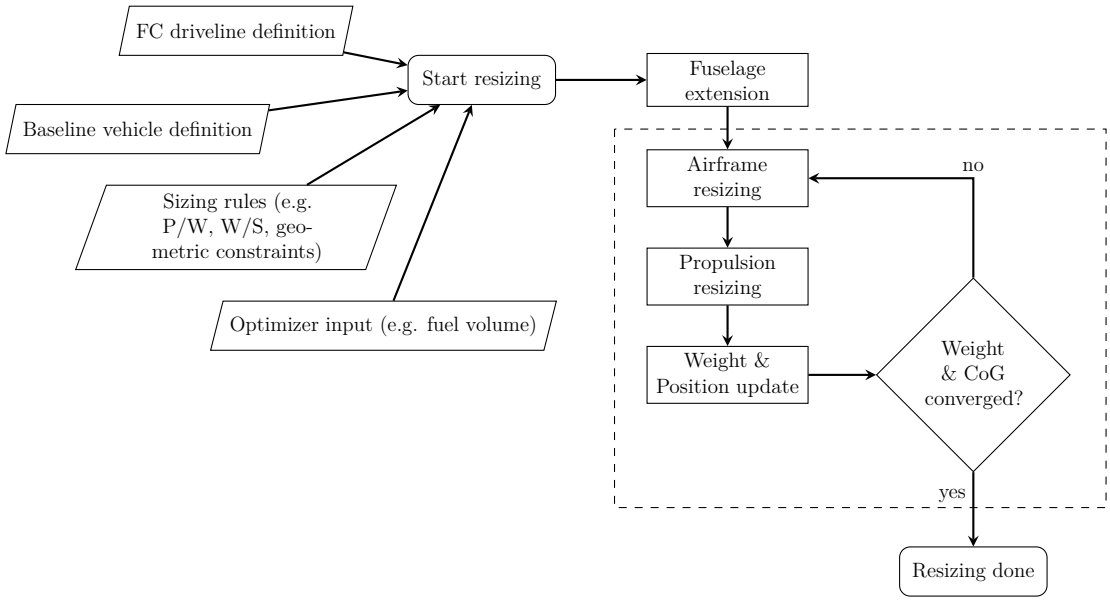

Figure 4.1: The iterative process of resizing a baseline aircraft.

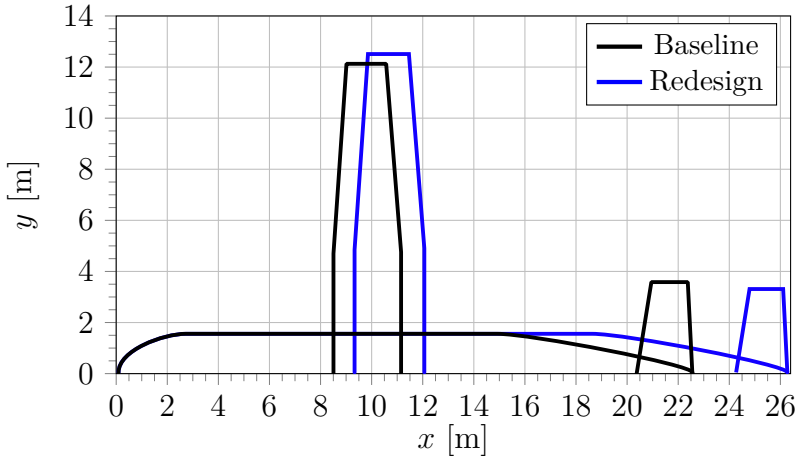

Figure 4.2: Example of planform resizing for an ATR 42 aircraft.

4.3 Mission simulation

The mission module in SUAVE is capable of simulating just about any type of flight mission. For simulating aircraft used in typical commercial operation, the simulated mission can be split into two parts: the intended flight to the destination, and a diversion. The flight to the destination will consist of a climb to cruise altitude, a cruise and finally a descent. At the destination, a loiter segment is performed in order to simulate the aircraft holding for landing. After this a diversion to an alternate airport is performed by climbing to (this time a lower) cruise altitude, cruising, and descending. At the alternate airport a final hold is performed by loitering, to account for final reserves. This type of mission, call it a design mission, is used to size the aircraft, as it accounts for all fuel that needs to be onboard. An illustration of the above described mission is seen in Figure 4.3.

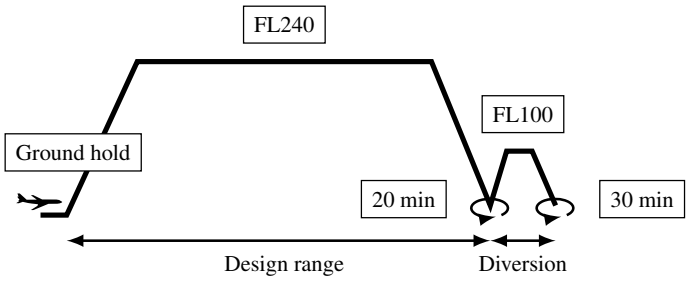

Figure 4.3: Design mission.

As is seen in the design mission, the combined horizontal distance of the first climb, cruise and descent make up the aircraft's design range. Off-design missions can involve flying faster or at different altitudes, or further if the payload is less. For conventional kerosene aircraft it is not uncommon for airlines to fill up with fuel at the origin, fly to the destination, and then back to the origin – all on the same fuel load. This is for economic reasons, as flying heavier and burning more fuel can be more profitable than filling up when the fuel prices are high. This could also be the

case for hydrogen aircraft, but it is more likely that this type of mission will be flown due to a future initial lack of hydrogen infrastructure. The boil-off performance of the cryogenic storage is then of high importance, as the fuel ventilated en-route and in turn-over will have a direct impact on the aircraft range. For these purposes a special "return-without-refuel"-mission can be set up, as seen in Figure 4.4.

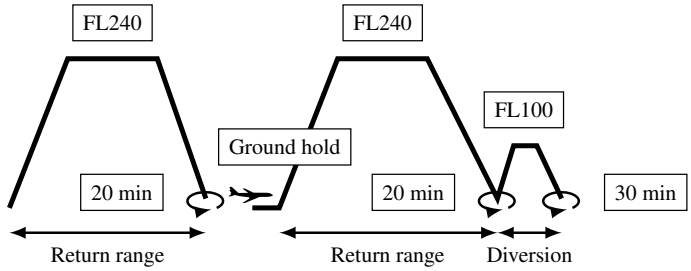

Figure 4.4: Return-without-refuel mission.

As seen in the return-without-refuel mission, there is only a reserve mission included for the return-leg, as it is assumed that an diversion occurring while flying to the destination will not allow for a return without refueling. The boil-off during turn-over at the destination is simulated in the "groundhold" segment, whereby the the tanks are subjected to no fuel mass flow and SL ambient temperature for a given amount of time.

4.3.1 Mission solver

The mission solver in SUAVE will solve the aircraft state (attitude and thrust-level) required to satisfy the motion prescribed by the individual mission segments. In each time step, the mission solver is fed the aircraft mass, which sets the amount of required lift force. With the prescribed dynamic pressure also known, SUAVE will solve for the resulting aircraft angle-of-attack (AoA). Using the dynamic pressure and now known required AoA, the resulting drag force is calculated. In steady-state conditions this drag force has to be countered with equal amounts of thrust force. The solver will then run the dynamic code for the thrust-making device, like an propeller, to solve for the required amount of propulsive power to generate the needed thrust. In the case of the airplanes considered in this work, the required power will then be the input to the fuel cell propulsion code, which will output the required mass flow of hydrogen back to the mission solver. The fuel flow is then added to the overall vehicle mass rate which is then integrated over mission time in order to decrease the vehicle mass. This whole process is highly interdependent, and therefore each aircraft state variable is iterated on using an optimizer-based approach, until there is force equilibrium in the vertical and horizontal directions.

4.3.2 Dynamic propulsion model

The dynamic propulsion model for the fuel cell aircraft consists of a fuel cell model and a thermodynamic model for the cryogenic storage. The fuel cell model will

iteratively solve for the current and resulting cell voltage that produces the total system power needed to satisfy the propulsive power demand. As mentioned before, this enables the calculation of the required fuel mass flow. This is then an input to the dynamic storage code, which is responsible for calculating the pressure inside the tanks. The fuel mass flow is an enthalpy outflow, which has a negative contribution to the pressure time derivative. The heat transfer is calculated according to the ambient conditions in the given mission solver time step, and has a positive effect on the pressure time derivative. These two energy flows work in opposite directions, and whether the pressure will increase or decrease will depend on the free stream conditions and power demand. When the pressure is at the ventilation pressure of the tank, the pressure time derivative has to be zero. This is done by ventilating gaseous hydrogen, which is a mass flow exiting the tank. Although relatively small, the venting mass flow will affect the performance of the aircraft, and is therefore an input to the mission solver's vehicle mass rate.

Chapter 5

Summary of papers

5.1 Paper 1

Hydrogen fuel cell aircraft for the Nordic market
C. Svensson, A. A.M. Oliveira, T. Grönstedt
International Journal of Hydrogen

5.1.1 Summary and discussion

In this paper a hydrogen fuel cell aircraft tailored for future Nordic air travel is sized and simulated. The Nordic region presents unique challenges such as long travel distances and sparse airport infrastructure, and therefore future demand on passenger volumes and travel distances were studied through a demand model. From this data, a range of 648 NM and a capacity of 50 passengers were set as design requirements for the aircraft. Using an ATR 42 turboprop as a baseline aircraft model, the PEMFC propulsion system and cryogenic storage were sized via new routines implemented in SUAVE. As the propulsive system and storage ended up increasing the MTOW of the baseline aircraft, an airframe resizing was required.

A parametric study of the cryogenic storage where the insulation thickness and ventilation pressure were varied showed small variations in the total design mission fuel consumption (fuel used and ventilated). An optimal tank, which balanced weight and boil-off performance, that minimized fuel burn was found to have a moderate ventilation pressure of $p_{max} = 1.76$ bar and an MLI layer count of 15. The performance of the MLI system was shown to be very effective, with a large part of the design space (MLI layer counts above 16) classified as infeasible, as tank pressure would drop below the fill pressure. Furthermore it was shown that maximizing GI was not optimal for this type of aircraft, as a very light tank will have excessive boil-off behavior.

Lastly four tank designs were run through the "return-without-refuel" mission. The tank with a high ventilation pressure and large MLI layer count ($p_{max} = 4.00$ bar, $N_{MLI} = 15$) was shown to perform the best when considering long groundhold times at the destination airport. This tank was able to be dormant for 10 hours at the destination without any significant inital range loss. For short groundhold times

(less than two hours), all tanks except the one with low ventilation pressure and low insulation layer count were able to achieve similar range performance.

5.1.2 Division of work

C. Svensson: Conceptualization, modelling, simulation, post-processing, data visualization, manuscript writing, manuscript reviewing

A. A.M. Oliveira: Consultation on fuel cell modelling, manuscript reviewing

T. Grönstedt: Conceptualization, manuscript writing, manuscript reviewing

5.2 Paper 2

Modelling hydrogen fuel cell aircraft in SUAVE
C. Svensson, P. Miltén, T. Grönstedt
34th Congress of the International Council of the Aeronautical Sciences (ICAS)

5.2.1 Summary and discussion

This paper presents methods for conceptually designing and simulating the mission performance of fuel cell aircraft in SUAVE. Routines for fuel cell system sizing, cryogenic storage sizing and airframe resizing are introduced. The fuel cell system design routine sizes the individual cells and arranges them into multi-stacks according to power needs and polarization curve characteristics. The air intake system, which includes the inlet, diffuser, compressor and turbine are sized using aerodynamic correlations and thermodynamic relations for a given worst-case operating point. The cooling system is sized to reject the maximum amount of heat produced by the fuel cell system, and uses the conceptual heat-exchanger design code GenHEX to design and evaluate the performance of the air-to-liquid heat-exchanger. The procedure for redesigning existing turboprop aircraft into fuel cell propulsion is also presented, where fuselage stretching, and wing and empennage resizing are presented. Correlation methods are used for defining the new aircraft weight, and the CoG is reassessed. Dynamic models used in the mission solving for calculating the PEMFC fuel mass flow and tank pressure are also presented.

A study on tank GI is performed in order to investigate the effect of total fuel volume and number of tanks. Here it is shown that for large fuel volumes, which will only fit in existing fuselage diameters if stored in cylindrical tanks, it is beneficial on GI to split the fuel into several smaller spherical tanks.

Finally a full resizing of an ATR 42 is performed using the iterative resizing loop. In order to fit 6 m^3 of fuel, the fuselage required a 16% stretch and the wing reference area was enlarged by 6% in order to maintain the original wingloading. Between MTOW and maximum zero fuel weight (MZFW) conditions, the CoG location moves 6% forward.

5.2.2 Division of work

C. Svensson: Conceptualization, modelling, simulation, post-processing, data visualization, manuscript writing, manuscript reviewing

P. Miltén: Creator of GenHEX conceptual heat-exchange design code, consultation on heat-exchanger design methods

T. Grönstedt: Conceptualization, manuscript writing, manuscript reviewing

Chapter 6

Conclusion

6.1 Concluding remarks

In this work the potential performance of hydrogen fuel cell aircraft for regional travel has been investigated. With its high efficiency, fuel cell propulsion shows great promise in offsetting the negative impact on energy use that liquid hydrogen storage brings to the performance of turboprop-style aircraft. The challenges it presents are the low specific power, large geometric footprint and large heat-rejection needs.

For the cryogenic storage it was demonstrated that the boil-off performance has a significant effect on the choice of tank design parameters. There is no clear answer on what the best tank design is, as lighter tanks perform the best in a normal design mission, while tanks with much worse GI perform better in the off-design. The available hydrogen refueling infrastructure and airline operations are therefore perhaps the ultimate deciding factors for the aircraft's performance, not overall tank weight or insulation effectiveness.

The fuel cell multi-stacks sized are representative for modern LT-PEMFC systems in terms of chemistry and system specific power. This has enabled us to investigate the cryogenic storage performance and needed modifications to the airframe. On the other hand, no aircraft have to this date flown with multi-stacks in the level of 2 MW, so there is a gap in the available data to perform proper validation of the full aircraft system-level performance. An experimental program has to deal with the problems that reality brings, and the predicted performance parameters such as system weight, volume and BoP overhead might therefore be subject to change.

To conclude this thesis, there is now a collection of design and mission performance models that have been integrated into SUAVE, that will be used to further refine the regional fuel cell aircraft concept and explore novel solutions to the challenges brought by this type of propulsion system.

6.2 Future work

To fully explore the performance implications that fuel cell propulsion systems bring to regional-type aircraft, further studies are needed. At the point of writing this, good routines for designing representative regional fuel cell aircraft have been implemented in SUAVE. With the performance of type 1 MLI tanks analyzed, it is of high interest to perform further studies on tanks with different insulation systems and pressure vessel materials. This could for example be a carbon fiber composite pressure vessel, which will improve on metallic tanks in terms of GI. It can also be of interest to study active heating systems inside the tank to prevent the pressure inside highly insulated tanks to drop below the fill pressure, which would expand the feasible design space in Paper 1.

For the fuel cell system specifically a study into different chemistries should be made in order to evaluate potential performance benefits compared to conventional LT-PEMFCs. A major downside of the low-temperature chemistries is the low temperature difference between the operating temperature and the ambient, which results in large required convection rates through the heat-exchanger. High-temperature PEMFC (HT-PEMFC) chemistries can remedy this, as operating temperatures can be substantially higher, but have been shown to perform worse in terms of cell power density and would therefore produce heavier multi-stacks. This trade is therefore of high interest.

It could also be of interest to look at investigating the performance trade of increasing or decreasing the maximum system voltage. Running the system at high voltage brings benefits such as decreased current through the electrical leads, which can then be downsized. It also has a direct effect on the amount of cells each stack has to contain. The risk involved with high voltages (around 1 kV and above) is the possibility of arc formation [42]. This is true for systems on the ground, but is of extra concern in aircraft as the insulative properties of air decreases with lowered density.

Finally we would like to investigate novel designs for the heat rejection system, in order to minimize the weight and aerodynamic drag of conventional heat-exchanger cooling ducts. This would use higher-fidelity modeling using computational fluid dynamics software, and system-level evaluation in SUAVE to quantify designs in terms of fuel burn.

Bibliography

[1] International Air Transport Association (IATA). *Airline Industry Economic Performance - October 2021 - Report*. 2021. URL: https://www.iata.org/en/iata-repository/publications/economic-reports/airline-industry-economic-performance---october-2021---report (cit. on p. 3).

[2] International Civil Aviation Organization via Airlines for America Processed by Our World in Data. *Global number of airline passengers*. 2023. URL: https://ourworldindata.org/grapher/number-of-airline-passengers (cit. on p. 3).

[3] International Council on Clean Transportation (ICCT) Brandon Graver. *Polishing my crystal ball: Airline traffic in 2050*. Accessed: 2024-11-13. 2022. URL: https://theicct.org/global-aviation-airline-traffic-jan22/ (cit. on p. 3).

[4] Hannah Ritchie. "What share of global CO emissions come from aviation?" In: *Our World in Data* (2024). https://ourworldindata.org/global-aviation-emissions (cit. on p. 3).

[5] International Air Transport Association (IATA). *Aircraft Technology Net-Zero Roadmap*. 2021 (cit. on p. 3).

[6] Jayant Mukhopadhaya and Brandon Graver. *Performance analysis of regional electric aircraft*. Tech. rep. ICCT, July 2022 (cit. on p. 3).

[7] Royal NLR – Netherlands Aerospace Centre. *Technological developments and radical innovations*. 2023. URL: https://www.nlr.org/focus-area/programmes/programme-climate-neutral-aviation/technological-developments-and-radical-innovations/ (visited on 09/13/2023) (cit. on p. 4).

[8] Abe Silverstein and Eldon W. Hall. *Liquid hydrogen as a jet fuel for high-altitude aircraft*. Research Memorandum NACA-RM-E55C28a. NACA, 1955 (cit. on p. 4).

[9] G D Brewer. *Hydrogen Aircraft Technology*. CRC Press, 1991 (cit. on p. 4).

[10] *Liquid Hydrogen Fuelled Aircraft – System Analysis*. Final Technical Report. Cryoplane project, 2003. URL: https://www.fzt.haw-hamburg.de/pers/Scholz/dglr/hh/text_2004_02_26_Cryoplane.pdf (cit. on p. 5).

[11] Reinhard Faaß. *CRYOPLANE Flugzeuge mit Wasserstoffantrieb*. Presentation. 2001. URL: https://www.fzt.haw-hamburg.de/pers/Scholz/dglr/hh/text_2001_12_06_Cryoplane.pdf (cit. on p. 5).

[12] Carlos Xisto and Anders Lundbladh. "Design and performance of liquid hydrogen fueled aircraft for year 2050". In: *International Council of The Aeronautical Sciences*. 2022 (cit. on p. 5).

[13] *Hydrogen-powered aviation – A fact-based study of hydrogen technology, economics, and climate impact by 2050*. Technical Report. Clean Sky 2 project, May 2020. URL: https://cleansky.paddlecms.net/sites/default/files/2021-10/20200507_Hydrogen-Powered-Aviation-report.pdf (cit. on pp. 5, 17).

[14] J. Hoelzen, M. Flohr, D. Silberhorn, J. Mangold, A. Bensmann, and R. Hanke-Rauschenbach. "H2-powered aviation at airports – Design and economics of LH2 refueling systems". In: *Energy Conversion and Management: X* 14 (2022), p. 100206. ISSN: 2590-1745. DOI: https://doi.org/10.1016/j.ecmx.2022.100206 (cit. on p. 5).

[15] Rompokos P., Rolt A., Nalianda D., Isekveren A. T., Senne C., and Grönstedt T. "Synergistic technology combinations for future commercial aircraft using liquid hydrogen". In: *Journal of Engineering for Gas Turbines and Power* 143.7 (2021) (cit. on p. 5).

[16] Brandon Graver, Rutherford Dan, and Zheng Sola. *CO_2 Emissions from Commercial Aviation: 2013, 2018, and 2019*. Tech. rep. ICCT, Oct. 2020 (cit. on p. 6).

[17] ZeroAvia. *Scaling hydrogen-electric propulsion for large aircraft*. Tech. rep. 2024. URL: https://zeroavia.com/download-scaling-h2-whitepaper/ (cit. on p. 6).

[18] *TYPE-CERTIFICATE DATA SHEET PW100 series engines*. 2023. URL: https://www.easa.europa.eu/en/downloads/7725/en (cit. on p. 6).

[19] ZeroAvia. *ZA2000*. URL: https://zeroavia.com/za2000/ (cit. on pp. 6, 7).

[20] Nieves Lapeña Rey, Jonay Mosquera, Elena Bataller, and Fortunato Ortí. "First Fuel-Cell Manned Aircraft". In: *Journal of Aircraft* 47.6 (2010), pp. 1825–1835. DOI: 10.2514/1.42234 (cit. on p. 7).

[21] Aerospace Technology. *HY4 Aircraft*. URL: https://www.aerospace-technology.com/projects/hy4-aircraft/ (cit. on p. 7).

[22] H2FLY. *H2FLY And Partners Complete World's First Piloted Flight of Liquid Hydrogen Powered Electric Aircraft*. URL: https://www.h2fly.de/2023/09/07/h2fly-and-partners-complete-worlds-first-piloted-flight-of-liquid-hydrogen-powered-electric-aircraft/ (cit. on p. 7).

[23] Universal Hydrogen. *Universal Hydrogen Successfully Completes First Flight of Hydrogen Regional Airliner*. 2023. URL: https://web.archive.org/web/20240523060649/https://hydrogen.aero/press-releases/universal-hydrogen-successfully-completes-first-flight-of-hydrogen-regional-airliner/ (cit. on p. 7).

[24] Universal Hydrogen. *Universal Hydrogen Successfully Completes First Flight of Hydrogen Regional Airliner*. 2024. URL: https://web.archive.org/web/20240815095823/https://hydrogen.aero/press-releases/universal-hydrogen-successfully-powers-megawatt-class-fuel-cell-powertrain-using-companys-proprietary-liquid-hydrogen-module/ (cit. on p. 7).

[25] ZeroAvia. *ZeroAvia Flight Testing Hydrogen-Electric Powerplant*. URL: https://zeroavia.com/flight-testing/ (cit. on p. 7).

[26] ZeroAvia. *ZA600*. URL: https://zeroavia.com/za600/ (cit. on p. 7).

[27] Anubhav Datta. *PEM Fuel Cell Model for Conceptual Design of Hydrogen eVTOL Aircraft*. Contractor Report NASA/CR-2021-0000284. NASA, 2021 (cit. on pp. 9–12, 14).

[28] A. Contreras, S. Yiğit, K. Özay, and T.N. Veziroğlu. "Hydrogen as aviation fuel: A comparison with hydrocarbon fuels". In: *International Journal of Hydrogen Energy* 22.10 (1997), pp. 1053–1060. ISSN: 0360-3199. DOI: https://doi.org/10.1016/S0360-3199(97)00008-6 (cit. on p. 15).

[29] Ian H. Bell, Jorrit Wronski, Sylvain Quoilin, and Vincent Lemort. "Pure and Pseudo-pure Fluid Thermophysical Property Evaluation and the Open-Source Thermophysical Property Library CoolProp". In: *Industrial & Engineering Chemistry Research* 53.6 (2014), pp. 2498–2508. DOI: 10.1021/ie4033999. eprint: http://pubs.acs.org/doi/pdf/10.1021/ie4033999 (cit. on p. 15).

[30] L Allidieris and F Janin. *Tanks (including insulation)*. Task Technical Report 3.6.2.1. Cryoplane project, 2002 (cit. on p. 16).

[31] Eytan J. Adler and Joaquim R.R.A. Martins. "Hydrogen-powered aircraft: Fundamental concepts, key technologies, and environmental impacts". In: *Progress in Aerospace Sciences* 141 (2023). Special Issue on Green Aviation, p. 100922. ISSN: 0376-0421. DOI: https://doi.org/10.1016/j.paerosci.2023.100922 (cit. on p. 17).

[32] D. Verstraete, P. Hendrick, P. Pilidis, and K. Ramsden. "Hydrogen fuel tanks for subsonic transport aircraft". In: *International Journal of Hydrogen Energy* 35.20 (2010). Hyceltec 2009 Conference, pp. 11085–11098. ISSN: 0360-3199. DOI: https://doi.org/10.1016/j.ijhydene.2010.06.060 (cit. on p. 17).

[33] Steven M Arnold, Roy M Sullivan, Jane M Manderscheid, and Pappu L N Murthy. *Review of Current State of the Art and Key Design Issues With Potential Solutions for Liquid Hydrogen Cryogenic Storage Tank Structures for Aircraft Applications*. Technical Memorandum NASA/TM-2006-214346. National Aeronautics and Space Administration, 2006 (cit. on p. 18).

[34] Frank P. Incropera, David P. Dewitt, Theodore L. Bergman, and Adrienne S. Lavine. *Incropera's Principles of Heat and Mass Transfer*. John Wiley Sons, 2017. ISBN: 9781119382911 (cit. on p. 18).

[35] Dries Verstraete. "The Potential of Liquid Hydrogen for long range aircraft propulsion". PhD thesis. Cranfield University, 2009 (cit. on p. 19).

[36] C. W. Keller, G. R. Cunnington, and A. P. Glassford. *Thermal Performance of Multilayer Insulations*. Contractor Report NASA/CR-1974-134477. NASA, 1974 (cit. on p. 19).

[37] Randall F Barron. *Cryogenic Systems*. en. 2nd ed. Monographs on Cryogenics. New York, NY: Oxford University Press, June 1985 (cit. on p. 20).

[38] Warren C Young, Richard G Budynas, and Ali Sadegh. *Roark's Formulas for Stress and Strain*. 8th ed. New York, NY: McGraw-Hill Professional, Dec. 2011 (cit. on p. 21).

[39] A. Wendorff et al. *SUAVE: An Aerospace Vehicle Environment for Designing Future Aircraft*. Version 2.1. 2020. URL: `https://github.com/suavecode/SUAVE` (cit. on p. 23).

[40] Trent Lukaczyk et al. "SUAVE: An Open-Source Environment for Multi-Fidelity Conceptual Vehicle Design". In: () (cit. on p. 23).

[41] Daniel P. Raymer. *Aircraft Design: A Conceptual Approach*. AIAA education series. American Institute of Aeronautics and Astronautics, 2018. ISBN: 9781624104909 (cit. on p. 23).

[42] Jordi-Roger Riba, Álvaro Gómez-Pau, Manuel Moreno-Eguilaz, and Santiago Bogarra. "Arc Tracking Control in Insulation Systems for Aeronautic Applications: Challenges, Opportunities, and Research Needs". In: *Sensors* 20.6 (2020). ISSN: 1424-8220. DOI: `10.3390/s20061654` (cit. on p. 34).